INVESTIGATING FUNDAMENTAL PROPERTIES OF WIND TURBINE WAKE STRUCTURE USING PARTICLE IMAGE VELOCIMETRY

J.Whale

Department of Mechanical Engineering
University of Edinburgh
Edinburgh EH9 4JL

Summary

Low Reynolds number flow visualisation tests are often used for showing the flow pattern changes associated with changes in lift-coefficients at a higher Reynolds number. In wind turbine studies, analysis of measured wake structures at small scale may reveal fundamental properties of the wake which will offer wake modellers a more complete understanding of rotor flows.

Measurements are presented from experiments on a model wind turbine rig conducted in a water channel. The laser-optics technique of Particle Image Velocimetry (PIV) is used to make simultaneous multi-point measurements of the wake flow behind small-scale rotors. Analysis of the PIV data shows trends in velocity and vorticity structure in the wake. Study of the flow close to the rotor plane reveals information on stalled flow and blade performance.

1 Introduction

A more detailed picture of the wake structure of a wind turbine is required if rotor design codes are to improve in terms of accurate performance prediction. There is evidence to suggest that even fundamental properties such as the shape of the wake boundary and the pitch of the wake spiral are not correctly modelled by current prediction codes(Montgomerie[3]).

Performing experiments in wind tunnels and water channels can provide much more detailed information concerning wake structure than tests at full-scale. Though the experiments are invariably conducted on reduced-scale models, it has been suggested that the fundamental properties of the wake may be independent of scale. Gould[2] states that the broader aspects of fluid flow patterns usually show much less change than the corresponding lift-coefficients over the same range of Reynolds numbers.

Since 1991, The University of Edinburgh has conducted tests on model wind turbine rotors using Particle Image Velocimetry (PIV). In these studies[e.g. 5], the technique of PIV has proved to be a quick, accurate and flexible method of obtaining detailed wake velocity measurements behind a model wind turbine, without the need for point probes or wires which disturb the flow.

The aim of this paper is to give an overview of the PIV tests at Edinburgh and to show the depth and range of information on wake parameters that can be obtained using the PIV technique.

2 Experiments

2.1 Laboratory Equipment

The experiments were performed with model wind turbine rotors of diameter 175mm. The set of rotors included simply-constructed flat-plate rotors of varying tip chord and linear taper as well as accurately-profiled replicas of full-scale machines, manufactured from rigid plastic by a professional model-maker[1].

---

[1] Angus Modelmakers, Glasgow

Figure 1 shows the model rig assembly. The turbine consists of 14W d.c. electric motor mounted on a platform. The rotors are attached to the turbine by means of a shaft which is connected to the electric motor by a toothed drive belt, housed in an aluminium tube.
The turbine rig is placed within a 10m long, 0.4m wide open water-channel filled to a depth of 0.75m. Steel rails running along the top of the channel support the frame of the rig, so that the platform is suspended above the water level and the aluminium tubing acts effectively as an inverted tower to the immersed rotor. A streamlined foam shroud was placed around the 'tower', to limit the interference of its wake with that of the rotor wake.
The speed and position of the rotor were measured by a tachogenerator and position encoder respectively, both connected to the electric motor. Output from the tachogenerator was supplied to a simple analogue speed controller which adjusted the drive motor to allow precise values of blade tip speed to be maintained. Output from the encoder was synchronised with the PIV recording equipment, so that flow records could be captured when the rotor blade reached a desired azimuthal angle.
A centrifugal pump supplied a steady recirculating current of 0.25m/s through the water channel. Turbulence manipulators were placed 7.5D upstream of the rotor to produce a uniform velocity profile with turbulence intensity levels of 4%. The speed of the electric motor was altered to change the blade tip speed in order to achieve the desired tip speed ratio. Tip speed ratios in the range $\lambda = 3 - 8$ were examined which corresponded to Reynolds numbers (based on chord length measured at 70% span) of 2600-16000.

2.2 PIV Facilities and Technique

Figure 2 shows a schematic diagram of the PIV system. The flow region is illuminated by an intense sheet of laser light, 2mm in thickness. The sheet-forming optics are housed within a metre long box, which runs on rails beneath the water channel. A rotating multi-faced mirror scans a high-powered laser beam onto a parabolic mirror which reflects the light sheet vertically upward through the glass base of the channel, highlighting a 2-d cross-section of the wake flow. The flow is seeded with 70um particles of conifer pollen which accurately follow the flow. Light scattered from the particles forms multiple-images on photographic film due to the stroboscopic illumination of the particles by the scanning laser. The film is subjected to a computer/optics based analysis that calculates the displacement of the recorded images in small local regions of the film. Thus, a complete grid of velocity vectors is formed and an instantaneous snapshot of the wake structure is produced.

An image-shifting system, consisting of a camera and a rotating mirror, is used to impose a translational velocity on all the recorded images, thereby resolving overlapping images corresponding to small particle displacements. This is similar to the approach of frequency shifting in Laser Doppler Anemometry (LDA) where a phase shifter is used to superimpose a known positive velocity on the measured velocities.

3 Results

A case study is presented. A 2-bladed flat-plate rotor with 1.26mm thickness, 15mm hub chord, 10mm tip chord and a linear taper was operated in the water channel at a tip speed ratio of $\lambda = 6$. The laser sheet illuminated a vertical cross-section of the flow past the model turbine, extending 3.5D in the axial direction and 2D in the cross-wake direction. Six photographs were taken each with the blade captured in the same azimuthal position; parallel to the tower of the rig. Thus the wake was recorded in the same phase and averaging of the flow records, subsequent to PIV analysis, served to extract the coherent structure in the wake from superposed turbulence.

The PIV negatives were analysed using three separate grids, focusing on different areas of the same negative. All dimensions are given in physical units i.e. actual distances in the water channel.

3.1 Full Near Wake: *3.5D × 2D area with 52 × 30 grid*

The velocity vector map of Figure 3 shows the wake as an area of reduced velocities behind the turbine. The wake can be divided into three distinct regions. Firstly, there is an *outer wake*, containing a strong vortex structure; evident from the sinusoidal pattern at the edge of the wake and attributed to the presence of vorticity shed from the tip of the blades. Secondly, there is a *wake core*, containing flow that appears to be almost stagnant immediately behind the nacelle. In addition, there appears to be a third region which bridges the gap between the outer freestream and the wake core; an '*inner wake*' that consists of a region of shear velocities.

The velocity data may be processed to produce vorticity contour plots. This gives a very visual picture of a 2-d slice through the wake as captured by the laser sheet. Figure 4 shows the tip vortices shed from the blades, embedded in areas of concentrated vorticity, either side of the wake centreline. These areas clearly indicate the shape of the wake boundary; an initial wake expansion is followed by signs of contraction at around 1.5D downstream. In the lower half of the wake, underneath the nacelle, it is possible to identify an area of strong vorticity corresponding to the region of sheared flow evident in Figure 3.

3.2 Half Near Wake: *2.75D × 1.4D area with 65 × 33 grid*

The PIV analysis was repeated on a finer scale, focusing on the lower half of the near wake where the effect of the tower wake on the recorded wake velocities was negligible. The velocity vector map of Figure 5 again depicts three distinct regions in the wake; a wake core and both an outer and inner wake. Further information is gained from the corresponding vorticity contour plot of Figure 6. Analysis on a finer scale resolves the areas of concentrated vorticity in the lower wake into discrete tip vortices. The contraction of the wake boundary at around 1.5D is clearly shown. The interaction of individual tip vortices is particularly noteworthy, with the coalescence of adjacent vortices at around 1.5D. Prior to this amalgamation, the preceding vortex looks to roll up over its neighbour and, at 2.5D, there are signs that the vortices dissociate after merging.

The root vortex can be seen in the top left hand corner of the contour plot. It appears to not be as strong as the tip vortices and dissipates after one revolution of the blade. The vorticity from the shear layer emanates from a region of the blade approximately 25-50% along the span from the hub and moves outboards under the influence of wake expansion to merge with the tip vortex system.

3.3 Rotor Plane Flow: *0.25D × 0.6D area with 18 × 42 grid*

PIV analysis of the same negative was carried out at a higher resolution once again, in order to highlight the region of flow very close to the rotor. This is shown in the vector map of Figure 7. The PIV experiments were not primarily designed to capture data at this level of resolution and consequently there are some areas of missing data and possible spurious vectors in Figure 7. The general patterns, however, of flow behaviour can be observed. The area behind the inner 35% of the blade appears to contain a lot of stagnant fluid whereas outboard of this region, the flow behind the blade contains larger flow velocities forming a much smoother flow pattern. This suggests that the inner 35% of the blade may be experiencing stall. The velocity vectors indicate an area of recirculating flow under the nacelle as well as a region of flow around the tip. The corresponding vorticity contour plot of Figure 8 shows these areas clearly as a root vortex which extends to the inner 30% of the blade and a tip vortex which forms at the last 20% of the blade.

4 Post-processing Analysis

The PIV velocity vector map and vorticity contour plot form the basis of all subsequent analysis. The following measurements were obtained from post-processing analysis of the PIV data and give an indication of the depth of information that can be provided by the PIV technique.

4.1 Mean axial velocity measurements

Analysing columns of vectors in the averaged velocity vector map of Figure 3 yields mean axial velocity profiles. In Figure 9, profiles are calculated at downstream distances of 0.5D to 2.5D at intervals of 0.5D. The highlighted profile at 0.5D displays the correct values of axial velocity ratio (mean axial velocity divided by freestream velocity) while the remaining profiles are offset by multiples of 0.25. The wake velocity profiles display an asymmetry around the centreline which can be attributed to the presence of the wake of the tower and is most prominent just behind the rotor. The high velocity deficits of the profiles (in some cases the axial induction values are close to unity) may be a consequence of low Reynolds number tests where viscous effects are relatively large, causing high drag on the rotor. With downstream distance, the profiles lose their depth as the wake recovers and the profile at 2.5D is seen to have a relatively flat central section.

Plotting the centreline velocity ratio with downstream distance shows the wake recovery process more clearly. Figure 10 plots the centreline velocity ratios for the case study $\lambda = 6$ alongside tip speed ratios of $\lambda = 3,4,5$ and 8. For each tip speed ratio, the curves show the slow-up of flow approaching the rotor, the jump in velocity value across the rotor plane and the gradual return to the freestream value. For the higher tip speeds of $\lambda = 5,6$ and 8, the graph shows centreline velocity ratios of negative value, immediately behind the rotor, suggesting areas of recirculating fluid within the wake. This is consistent with behaviour observed in the *turbulent wake state*, as defined by Eggleston &Stoddard[1]. A movement of fluid across the shear layer into the wake core may explain the contraction of the wake (due to conservation of mass flux) and the uniformity of wake profiles, observed from the PIV results.

4.2 Tip vortex measurements

The vorticity contour plots can be used to give quantitative values of tip vortex properties. Identifying each discrete tip vortex in Figure 6 by positions of maximum vorticity, the axial spacing of the tip vortices can be calculated. Figure 11 shows a plot of axial downstream position for each tip vortex for tip speed ratios of $\lambda = 3,4,5,6$ and 8. The graph shows that axial spacing decreases with λ in accordance with a decrease in the helix angle of the tip vortex system. It is noteworthy that, for both the cases $\lambda = 6$ and 8, there is suggestion of an increase in tip vortex spacing after around 4-5 blade revolutions. It may be plausible that, although the helix system is initially densely packed behind the rotor, the recirculating flow causes an acceleration of the tip vortices so that, further downstream, the packed vortex spiral becomes less compressed. One must be careful in drawing firm conclusions from the graph, however, due to the small number of datapoints.

The value of the maximum vorticity, used to identify tip vortices, may be plotted against downstream distance to give an indication of tip vortex strength and decay in the wake. Figure 12 shows that there appears to be more energy in the tip vortex system as λ increases. This is consistent with full-scale smoke studies[4] . A number of factors may influence the strength and lifetime of a tip vortex, however, and it is difficult to draw conclusions on the basis of tip speed ratio alone.

4.3 Mean radial flow measurements

In addition to axial velocity measurements, the PIV velocity vector maps allow analysis of velocities in a radial direction. Figure 13 shows the radial flow for the velocity vectors in Figure 7 by analysing the column of vectors either side of the blade. The graph shows that near the tip of the blade, there is a dramatic increase in outward flow on the pressure surface of the blade and a corresponding increase in the inward flow on the suction surface of the blade. This behaviour is consistent with the existence of strong vortex around the tip of the blade. The inner 20-50% of the blade depicts outward flow on both the pressure and suction surfaces of the blade. This can be attributed to centrifugal forces on the blade.

The PIV velocity measurements, together with the corresponding vorticity values can be used to obtain detailed information about blade performance, notably the spanwise distribution of lift and angle of attack, as presented in Figure 14. The lift distribution across the blade is obtained by firstly using the strength of the trailing vorticity (captured in the PIV experiments as it is shed from the blade) to calculate the change in bound circulation and then applying the Kutta-Joukowski law. The lift distribution presented in Figure 14 seems encouraging though the values of lift coefficient are slightly higher than expected for the low Reynolds number tests. The distribution suggests that the inner 35% of the blade is stalled which is consistent with the vector map of Figure 7.

Using the ratio of the axial component of velocity to the blade tip speed at sections along the blade, the spanwise distribution of angle of attack may be computed. The graph shows an increase in α at the tip which may be the effect of the tip vortex. The blade appears to be experiencing stall for angles greater than 10° and a larger region of the blade is stalled than would be expected at full-scale. This result is consistent with the low Reynolds numbers of the experiments.

5 Errors

The PIV experiments described in this paper contain a number of sources of error, many of which, when quantified, can be treated as negligible. A study of the influence of the walls of the water channel on the flow past the model rotor produced an estimate of correction for blockage of 2.5%. The combined systematic error from the PIV technique contributed less than 3% error in velocity measurement and random errors were responsible for 1% error. Errors in velocity measurement were compounded during vorticity calculations. The maximum error in vorticity, however, was estimated as 6%.

The most important concern is that of scale effect since the blade Reynolds number of the PIV tests was lower than full-scale by a factor of 1000. It is likely that there would be a difference in the phenomena of separation and re-attachment at the blade compared to full-scale, which may be conveyed to the wake structure. The same phenomena of circulatory lift and trailing vorticity occur on wind turbine blades at all scales, however, and although detailed full-scale wake flow may differ from that observed at model scale, there is a strong possibility that there will be fundamental similarities.

6 Conclusions

The method of PIV was used to make global observations concerning the near wake structure of a model wind turbine, operating in a water channel. A 2-blade flat-plate rotor operating at a tip speed ratio of $\lambda = 6$ was used as a case study.

The study showed wake behaviour affecting the fundamental geometry of the vortex spiral. Interaction between tip vortices in the helical vortex system led to a breakdown of vortex structure and the shape of the wake boundary was seen to contract further downstream. There were also signs that this coincided with an increase in helix pitch angle and together the

evidence suggests that the packed vortex spiral immediately behind the rotor forms a barrier separating inner and outer wake. Once the barrier has weakened, through vortex interaction and decay, there is re-entrainment of the freestream into the wake with the resulting contraction and acceleration of the spiral. One must be careful in drawing firm conclusions from this one case study and further data is required to support this theory. It is clear, however, that the current BEM model is fundamentally flawed in the assumption of asymptotic slow-down of the wake behind the rotor.

The PIV velocity vector maps and vorticity contour plots revealed a region of sheared flow between the tip vortex system and the wake core. The stretching of smoke filaments inboard of the tip in smoke studies by Pedersen & Antoniou[4] support the existence of a shear layer at full-scale. It is likely that this region is exaggerated in the low Reynolds number tests due to a relatively thick boundary layer on the model blades.

Although the PIV experiments were not designed to capture detailed flow over the blades, analysis of a section of the PIV negative close to the rotor plane produced very encouraging results. Clear trends in flow patterns were identified, corresponding to tip and root vortex structure as well as areas of stalled flow. The results were analysed to produce a lift-coefficient distribution over the blade which, in the absence of thrust and torque measurements on the rotor, gave insight into blade performance. Research into stalled flow remains a priority for workers in the wind turbine industry. There is a lack of airfoil data for use in combination with BEM, particularly for incidences beyond stall. PIV has the advantage of making direct measurements of the local angle of attack and a further set of PIV experiments, focusing on the rotor plane would be very interesting.

The potential of the PIV method in obtaining detailed information concerning wake structure is clear and the author believes that a comprehensive set of PIV measurements would have a great deal to offer to wake modellers looking to gain insight into the fundamental physical processes governing wake behaviour.

Acknowledgements

The author is extremely grateful for the support and advice given by Colin Anderson of Aerpac U.K. and Tom Bruce of the University of Edinburgh.

This project is funded by the Engineering and Physical Sciences Research Council.

References

[1] EGGLESTON, D. M. & STODDARD, F. S. 1987 *Wind Turbine Engineering Design*, Chapter 1, pp 30-35, Van Nostrand Reinhold.

[2] GOULD, R. W. F. 1968 Design of a low-speed water channel. *NPL AeroReport*, pp 2 -3.

[3] MONTGOMERIE, B. 1990 The need for more measurements. *Proceedings of the 4th International Energy Agency (IEA) Aerodynamics Symposium*, Rome, Italy.

[4] PEDERSEN, T. F. & ANTONIOU, I. 1989 Visualisation of flow through a stall-regulated wind turbine rotor. *Proceedings of the 1989 European Wind Energy Conference*, Glasgow, Scotland, 83-89.

[5] WHALE, J., BAREIß, R., WAGNER, S. & ANDERSON, C. G. 1996 The wake structure of a wind turbine - comparison between PIV measurements and free-wake calculations. *Proceedings of the 1996 European Union Wind Energy Conference*, Göteborg, Sweden, 457-460

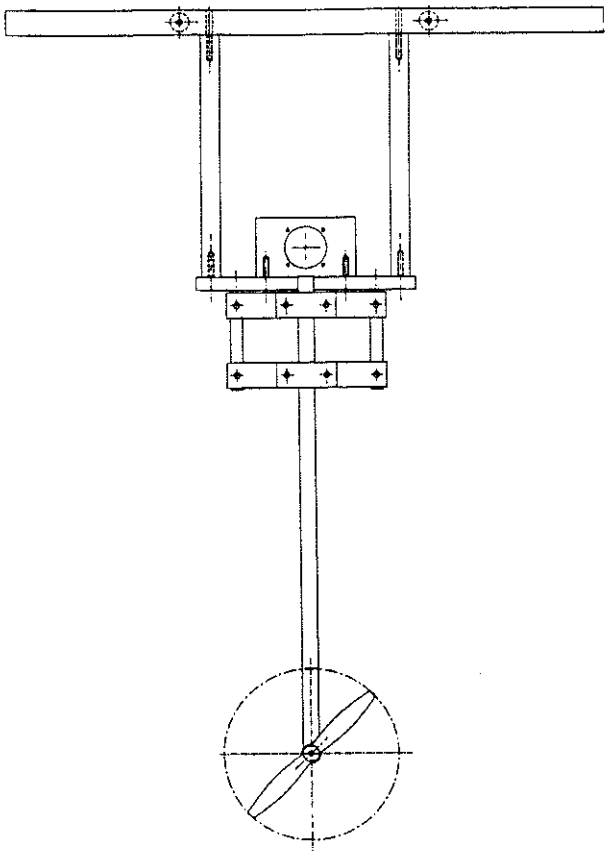

Figure 1 Assembly drawings of the model turbine rig

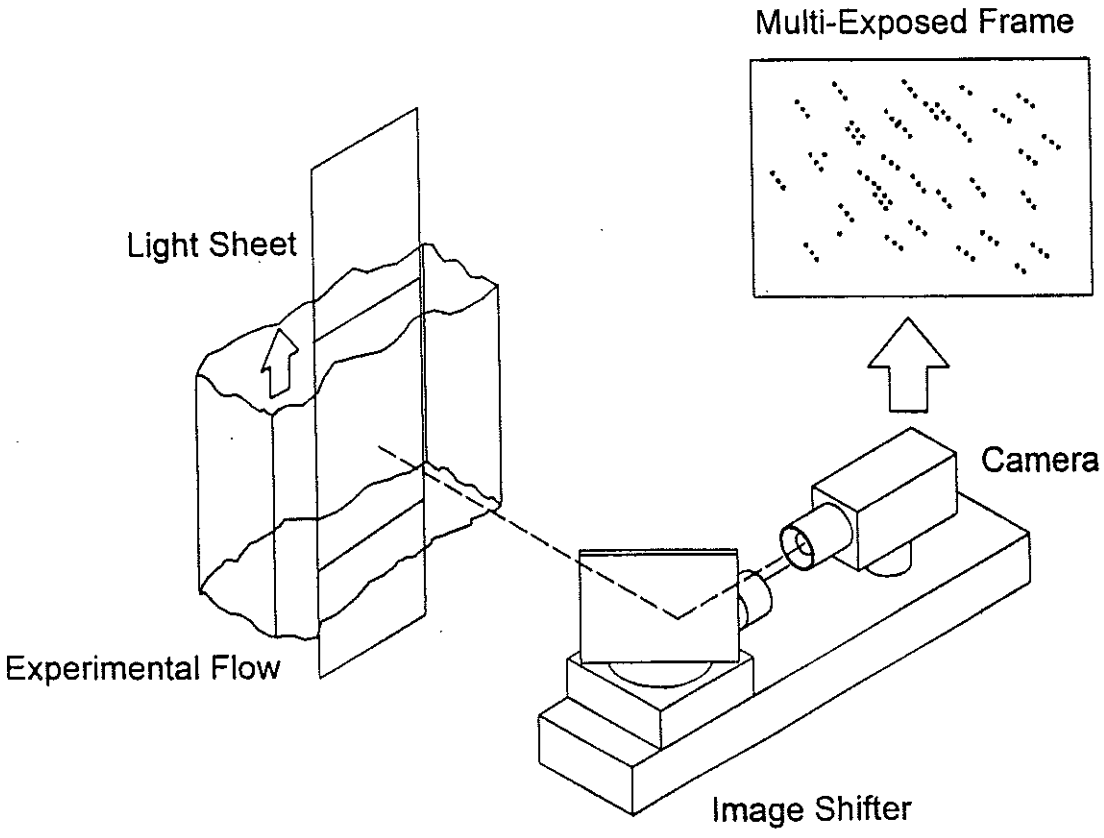

Figure 2 Schematic diagram of the PIV system

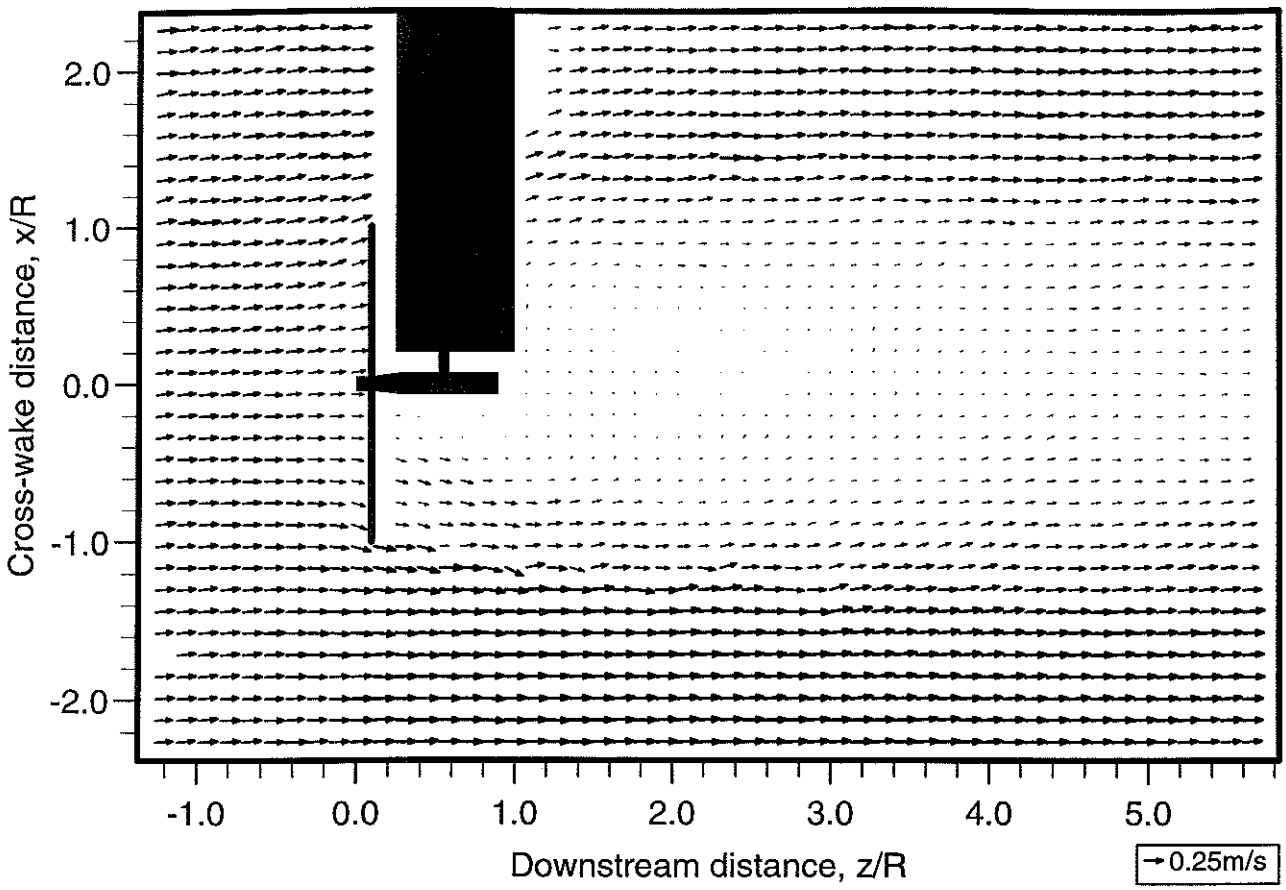

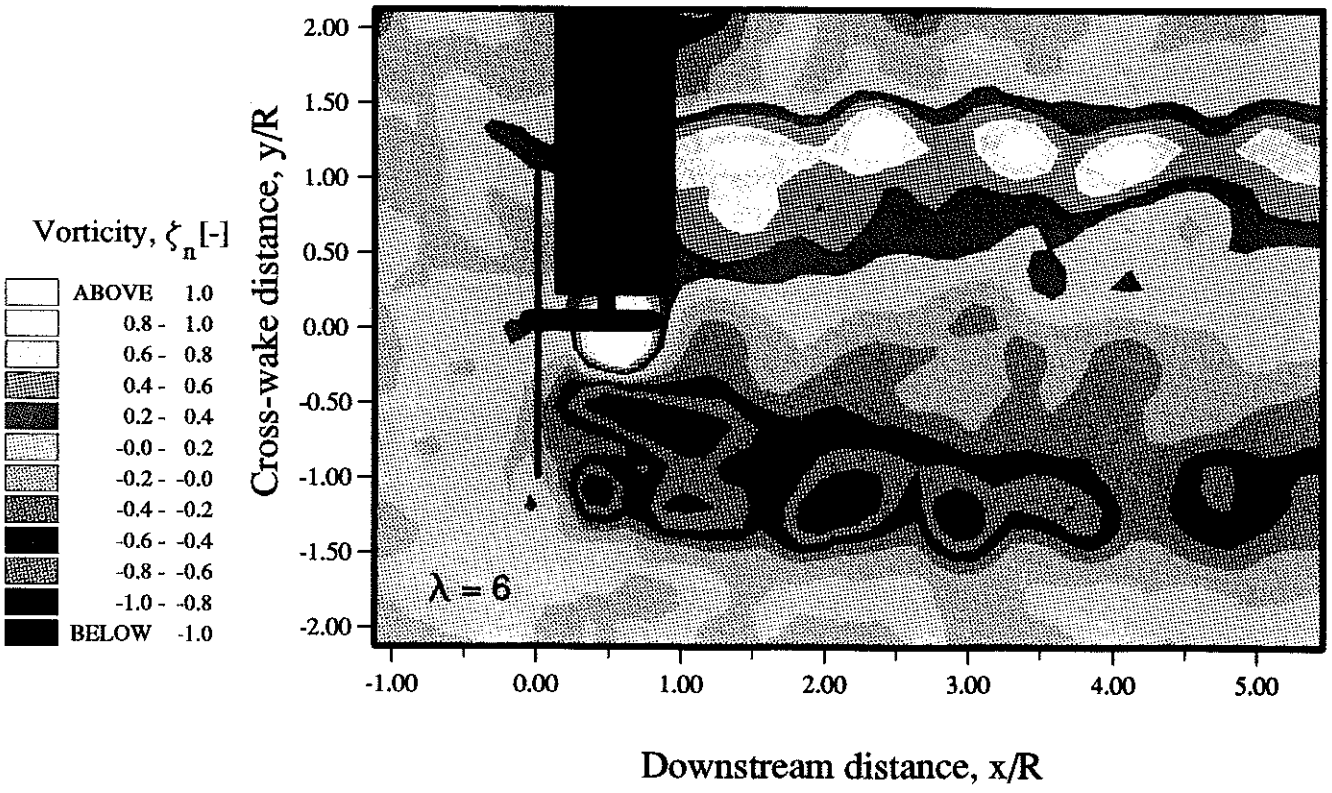

Figure 3 PIV data in the near wake

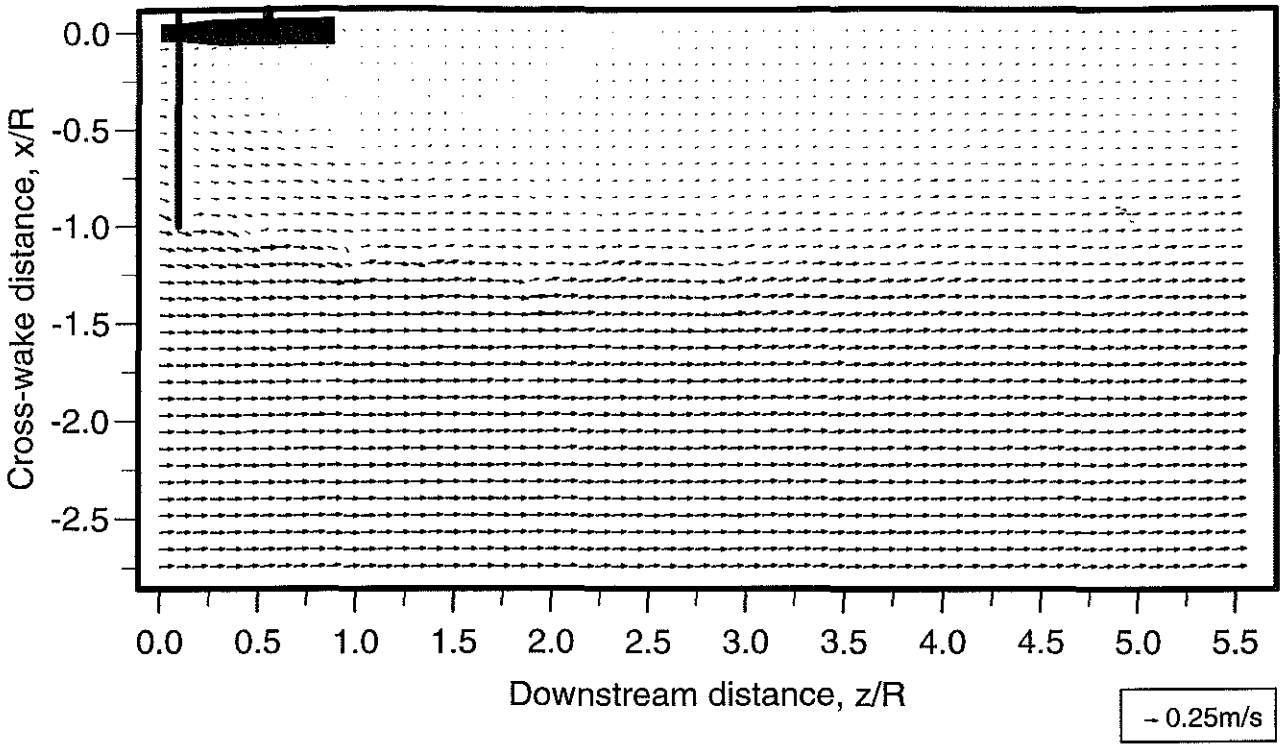

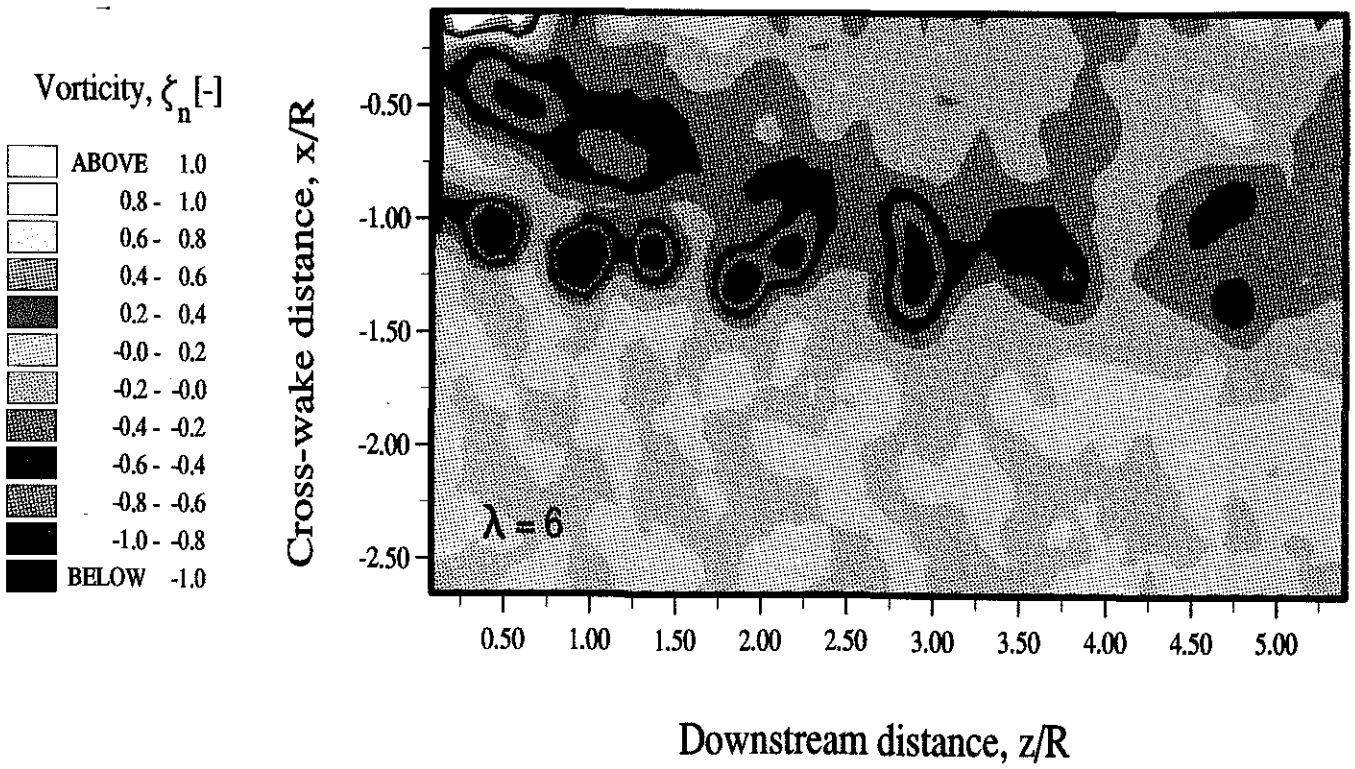

Figure 6 PIV data in the lower half of the wake

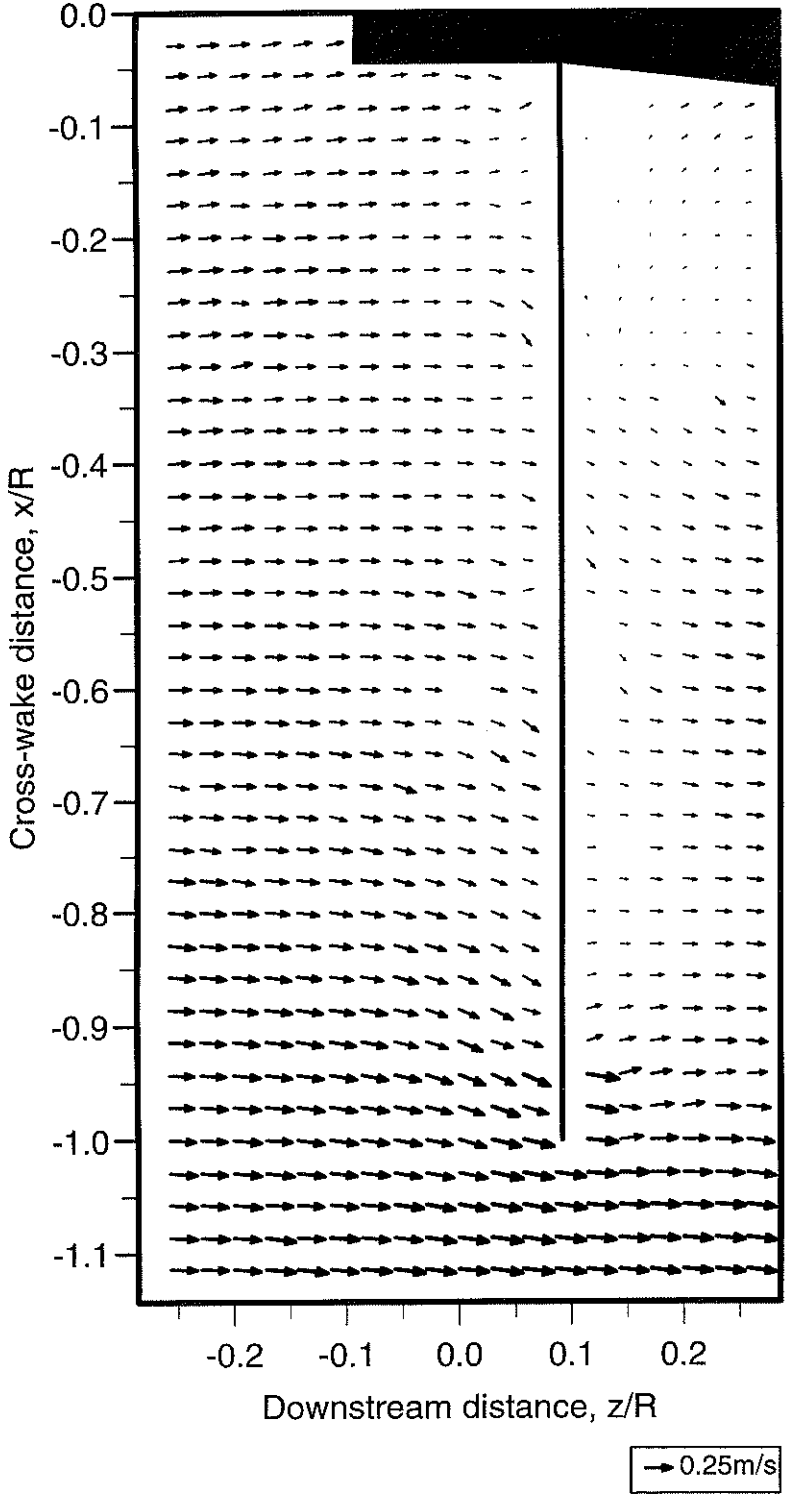

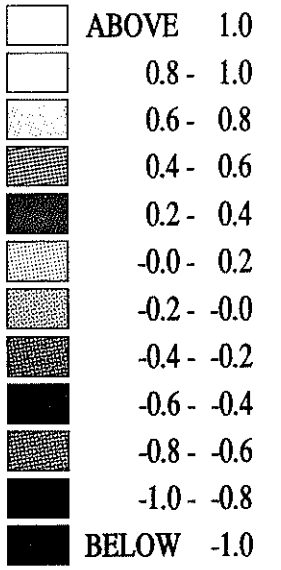

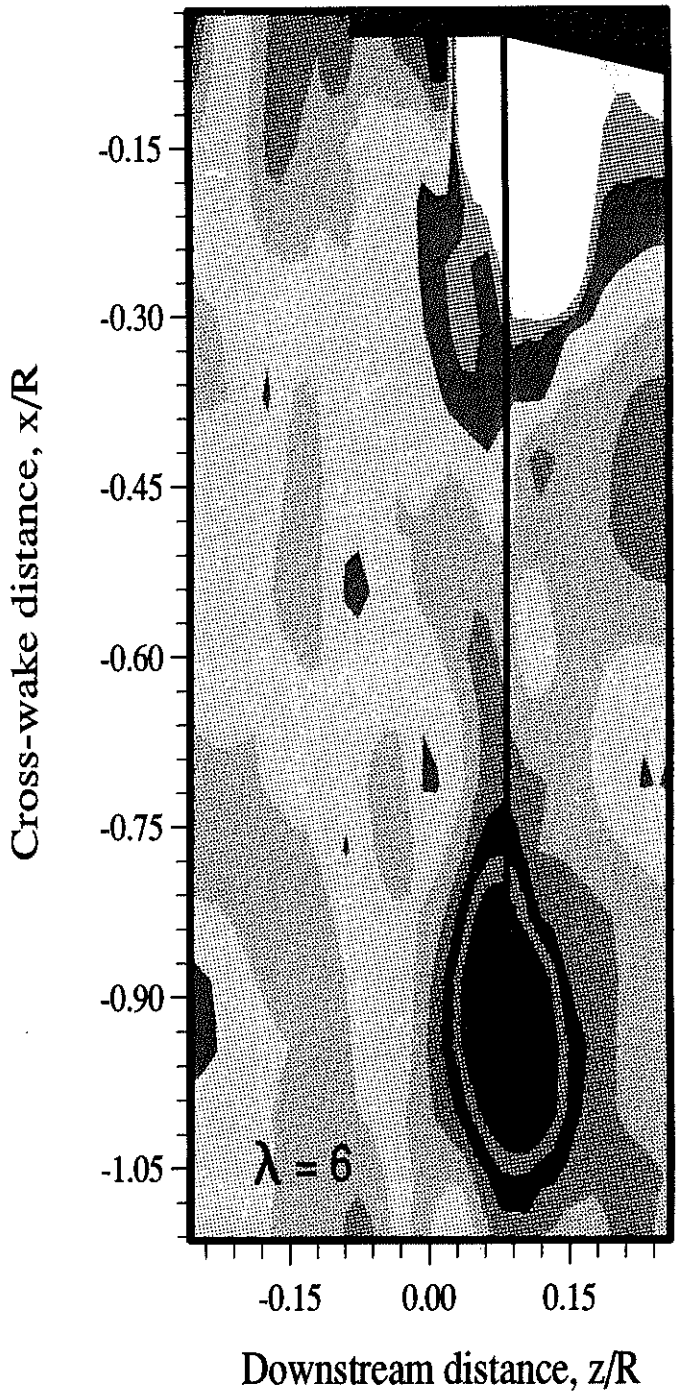

Figure 9 PIV data close to the rotor plane

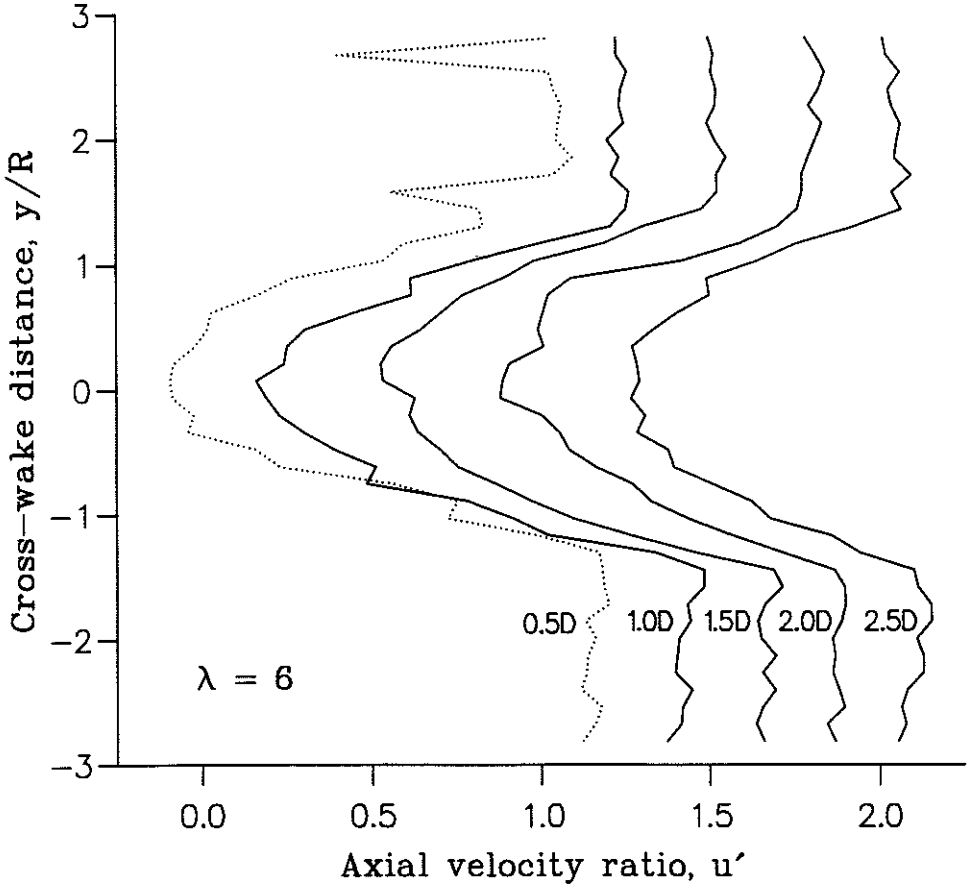

Figure 4 PIV velocity profiles in the wake

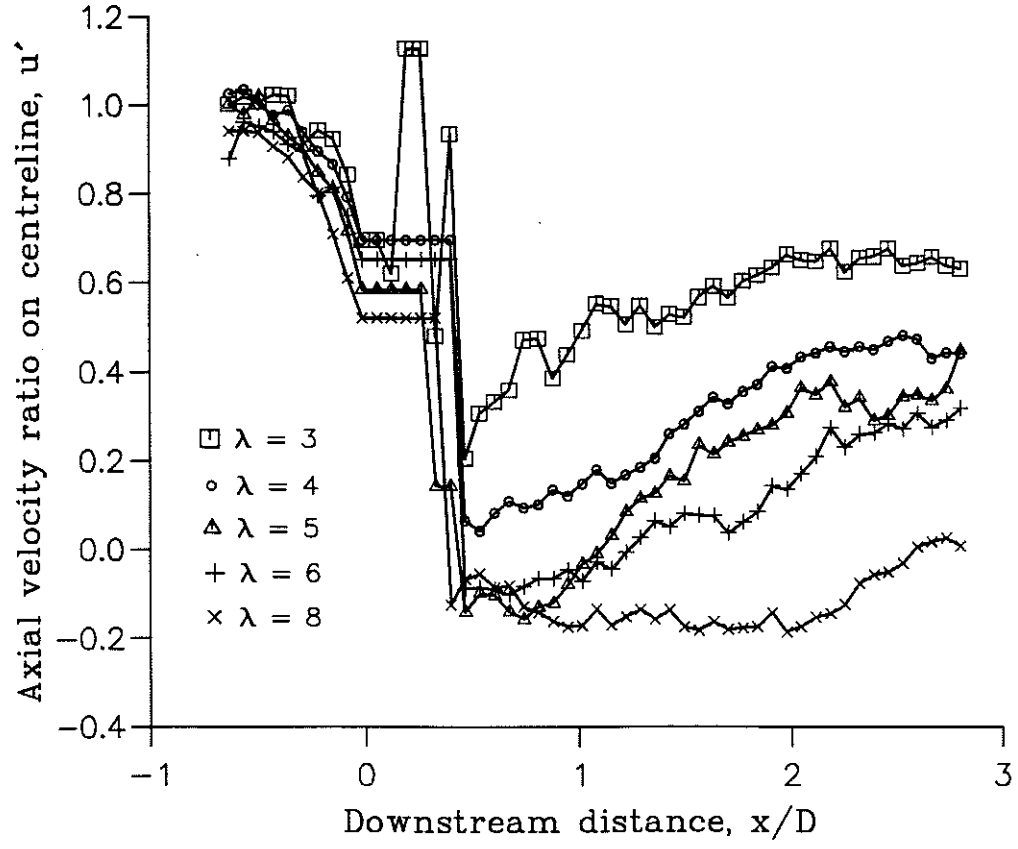

Figure 5 Centreline velocity ratios in the wake

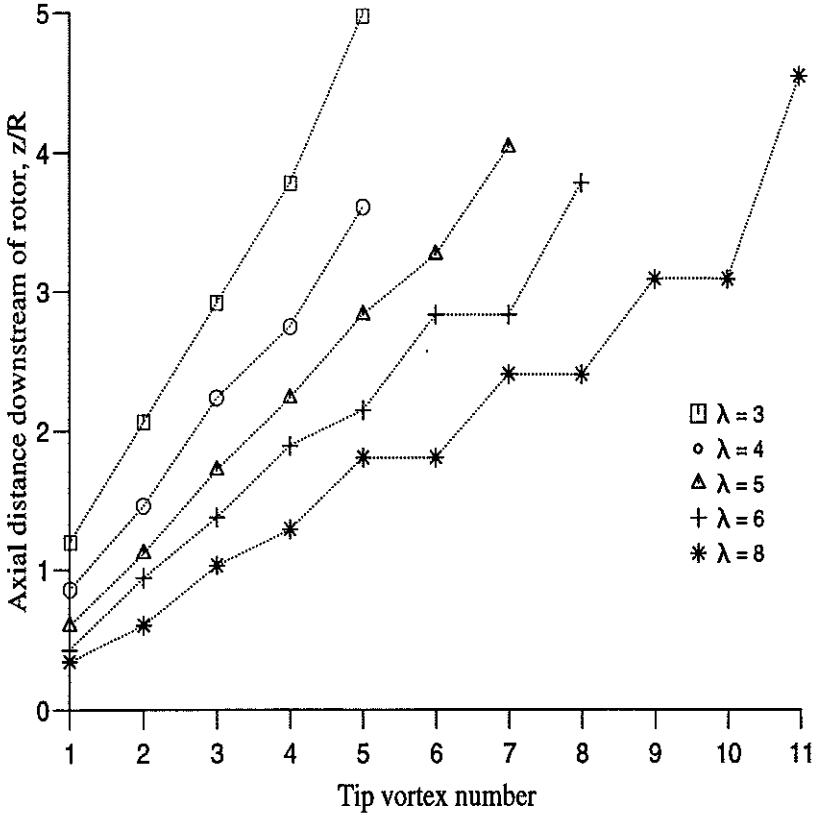

Figure 11 Axial spacing of the tip vortices

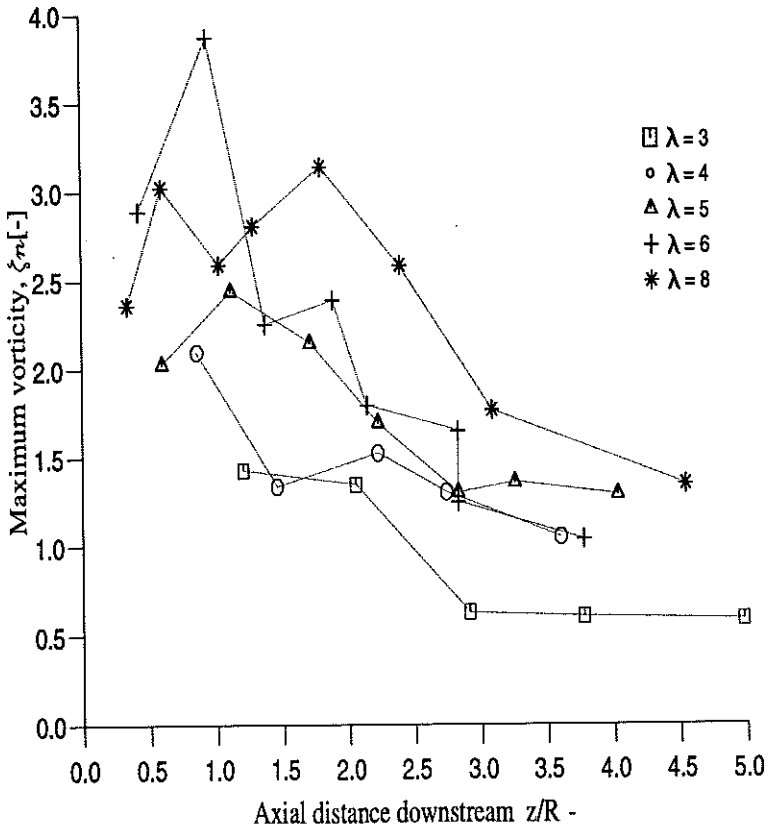

Figure 12 Strength of the tip vortices

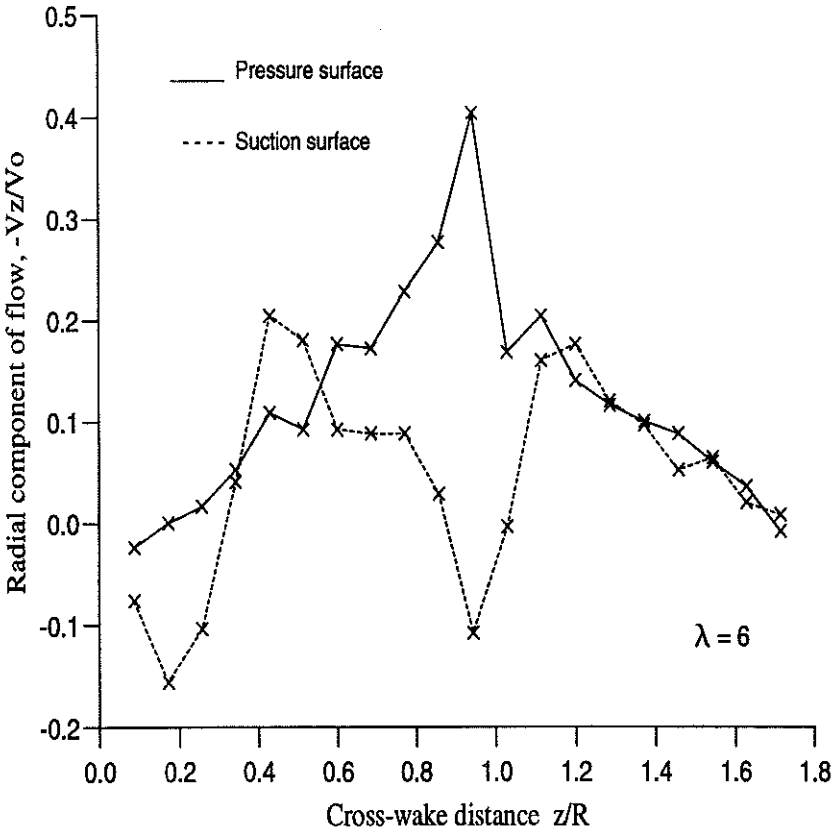

Figure 13 Radial flow at the rotor plane

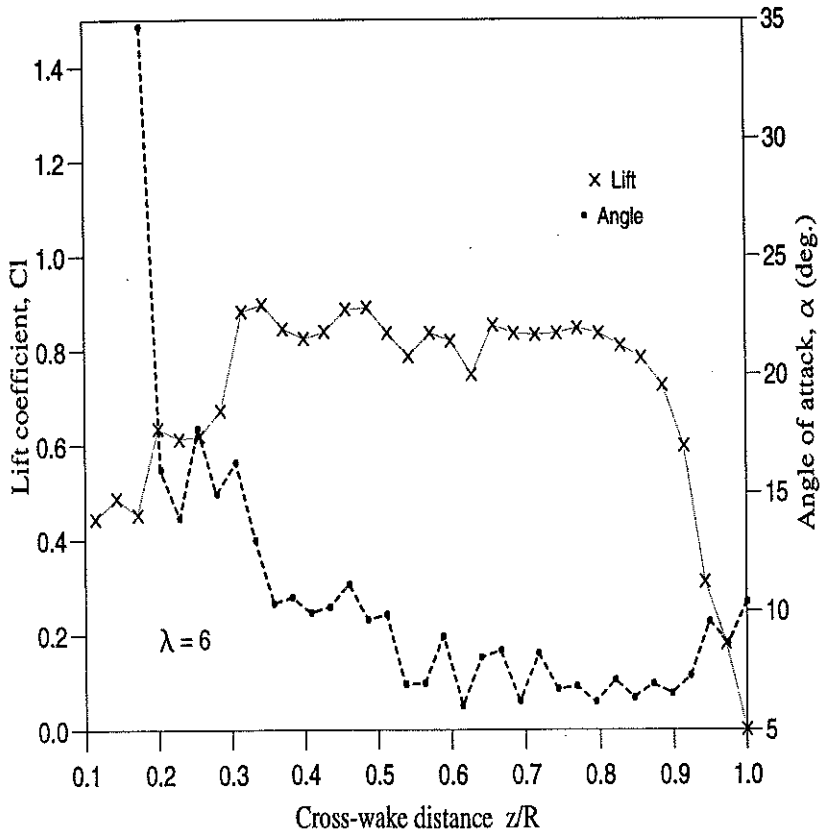

Figure 14 Spanwise distributions of lift and angle of attack